Controllable Synthesis of Conjugated Thiophenylethyne-based Compounds with Different Chain Lengths

Wei Huang, Haoyun Zhu, Yuli Huang, Junwei Yang and Weizhi Wang*

State Key Laboratory of Molecular Engineering of Polymers, Department of Macromolecular Science, Fudan University, Shanghai 200433, P. R. China. E-mail: weizhiwang@fudan.edu.cn; Tel: +86 021-65643836

Supporting Information

Table of Content

Table S1 Summary of crystal data and reflective collection parameters for **2**.

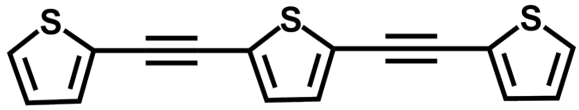

Empirical formula	$C_{16}H_8S_3$
Formula weight	296.40
Crystal size, mm	0.26 x 0.21 x 0.17
Crystal system	Monoclinic, C2/c
space group	P2(1)/c
a, Å	15.042(5)
b, Å	11.404(4)
c, Å	c = 32.856(10)
a, deg	90
β, deg	95.094(5)
γ, deg	90
V, $Å^3$	5614(3)
Z	16
Calculated density, Mg/m^3	1.403
F(000)	2432
Temperature, K	296(2)
Wavelength, Å	0.71073
μ(Mo Ka), mm^{-1}	0.509
$2\theta_{max}$,deg (Completeness)	25.00 (98.5 %)
no. of collected reflections	13829
no. of unique ref.(R_{int})	4882 (0.0618)
Data/restraints/parameters	4882 / 7 / 352
R_1, wR_2 [obs $I>2\sigma$ (I)]	0.0881, 0.1980
R_1, wR_2 (all data)	0.1181, 0.2094
residual peak/hole, e. $Å^{-3}$	0.634 / -0.752
transmission ratio	0.9185/ 0.8791
Goodness-of-fit on F^2	1.067

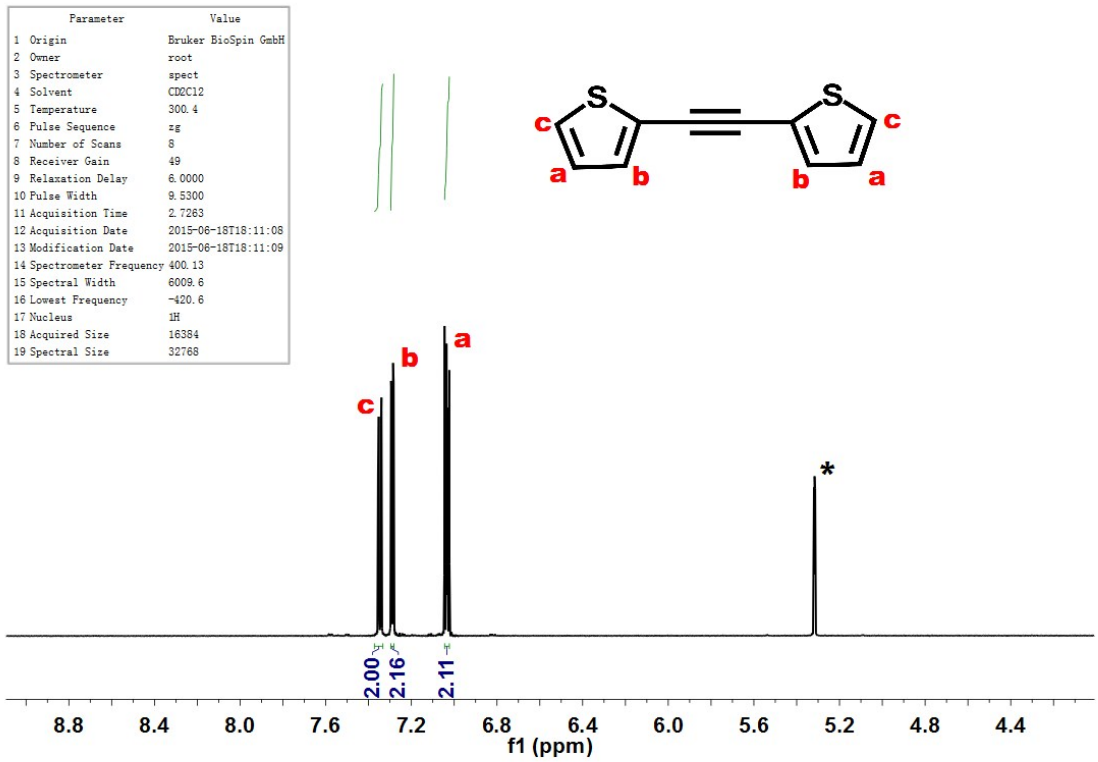

Fig. S1 The ^{1}H NMR spectrum of **1**.

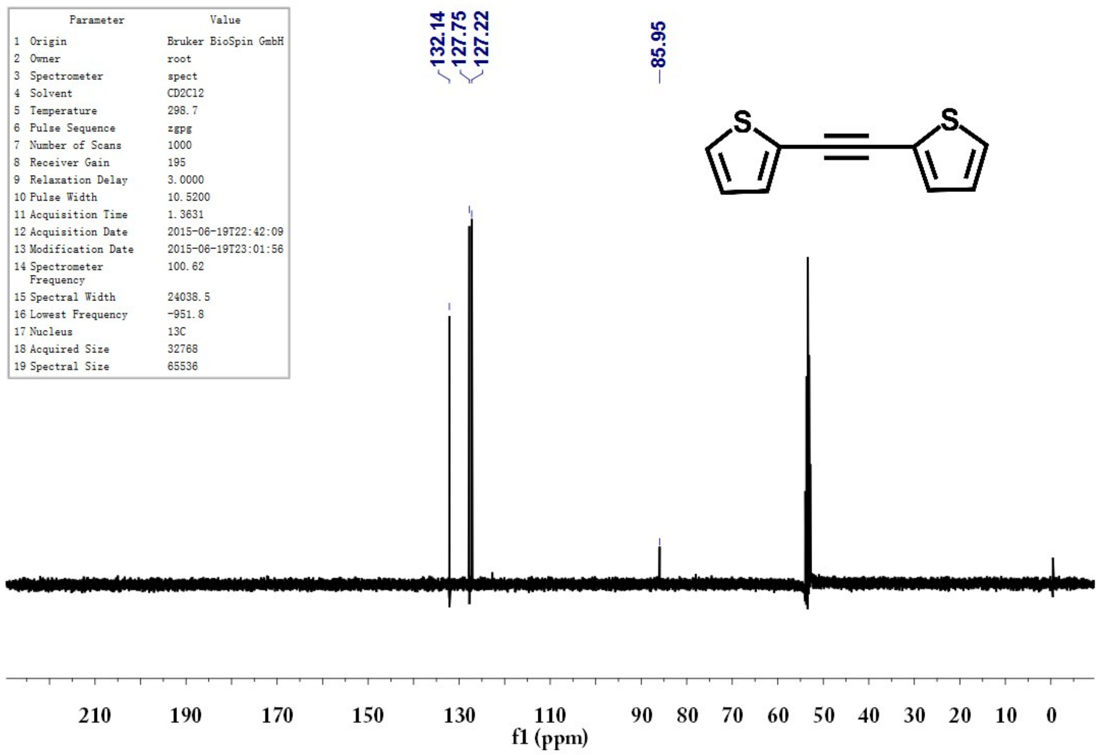

Fig. S2 The ^{13}C NMR spectrum of **1**.

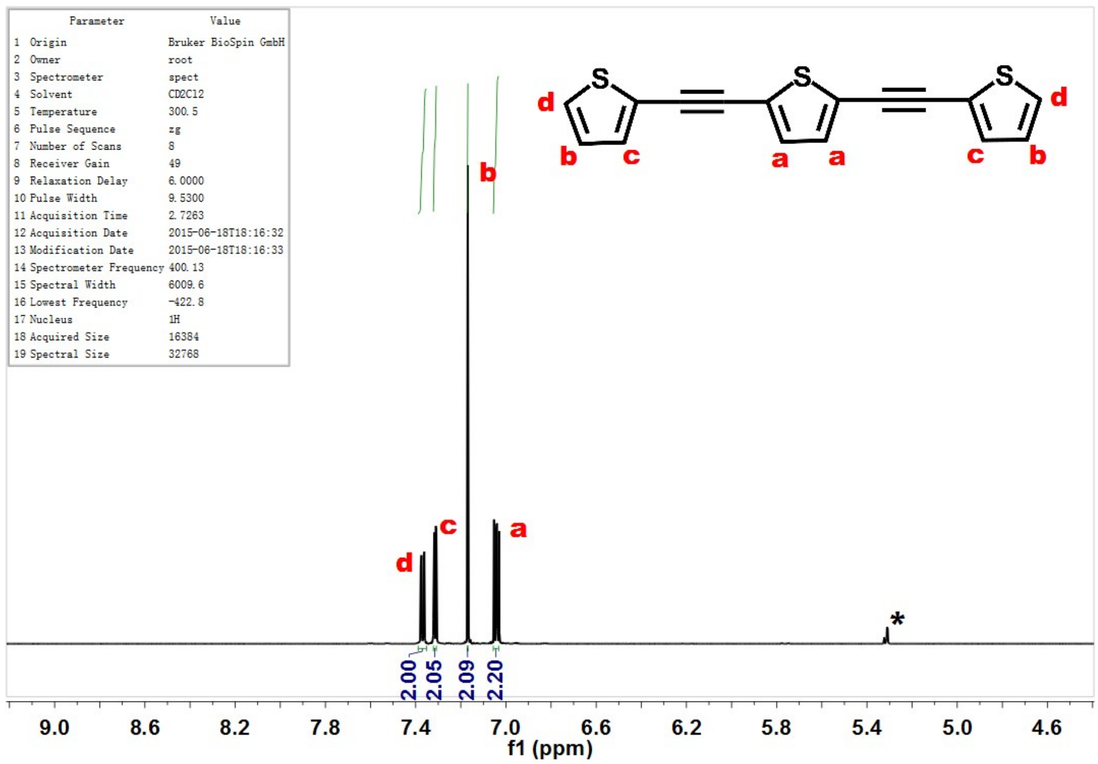

Fig. S3 The ^{1}H NMR spectrum of **2**.

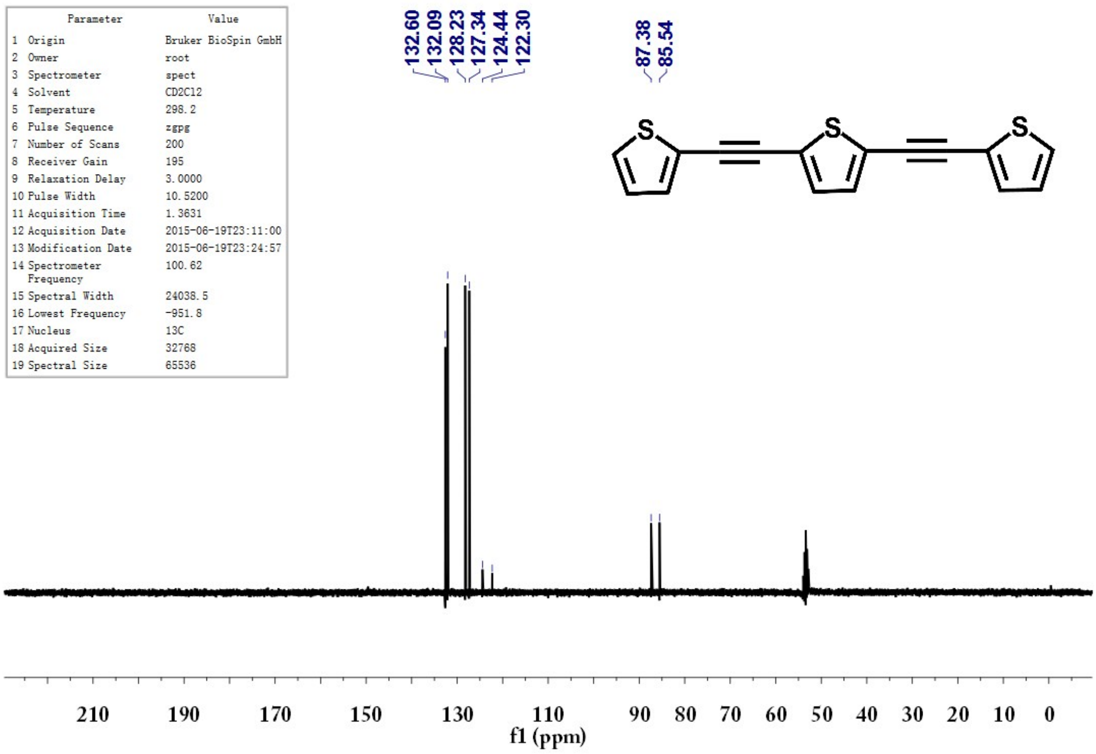

Fig. S4 The ^{13}C NMR spectrum of **2**.

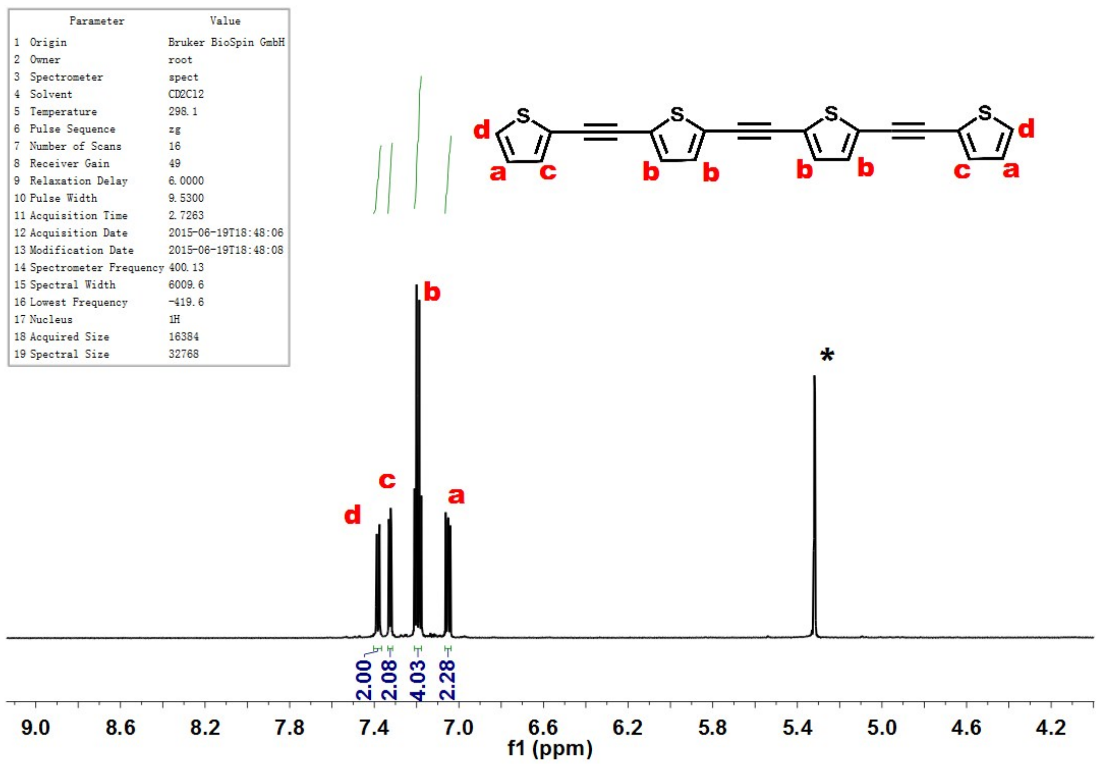

Fig. S5 The ^{1}H NMR spectrum of **3**.

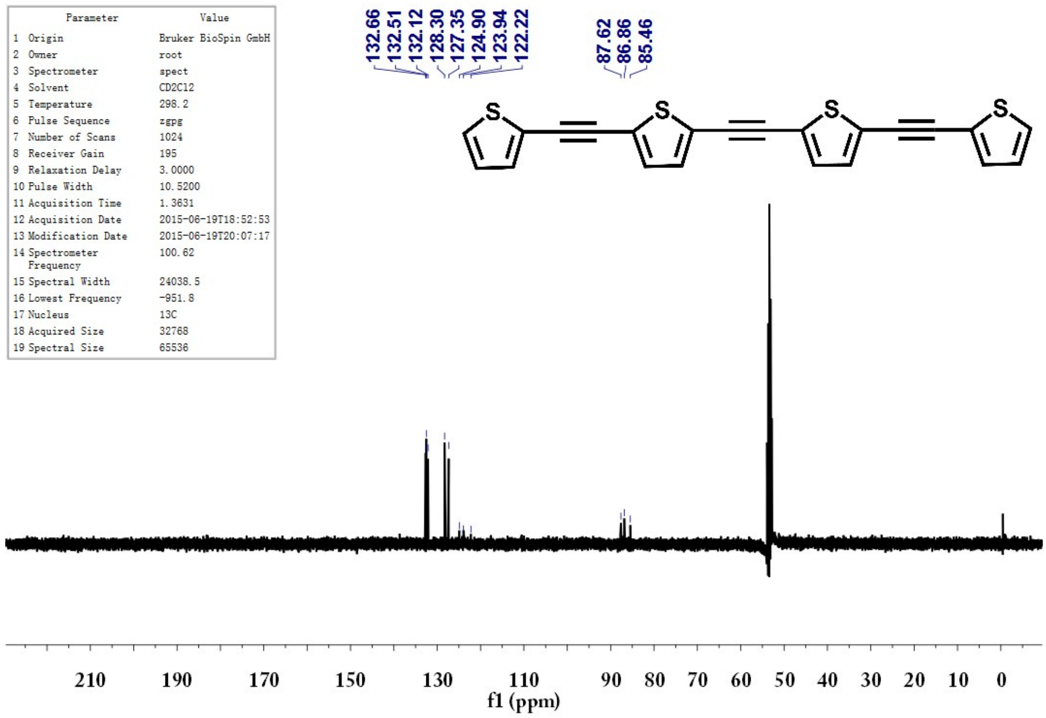

Fig. S6 The ^{13}C NMR spectrum of **3.**

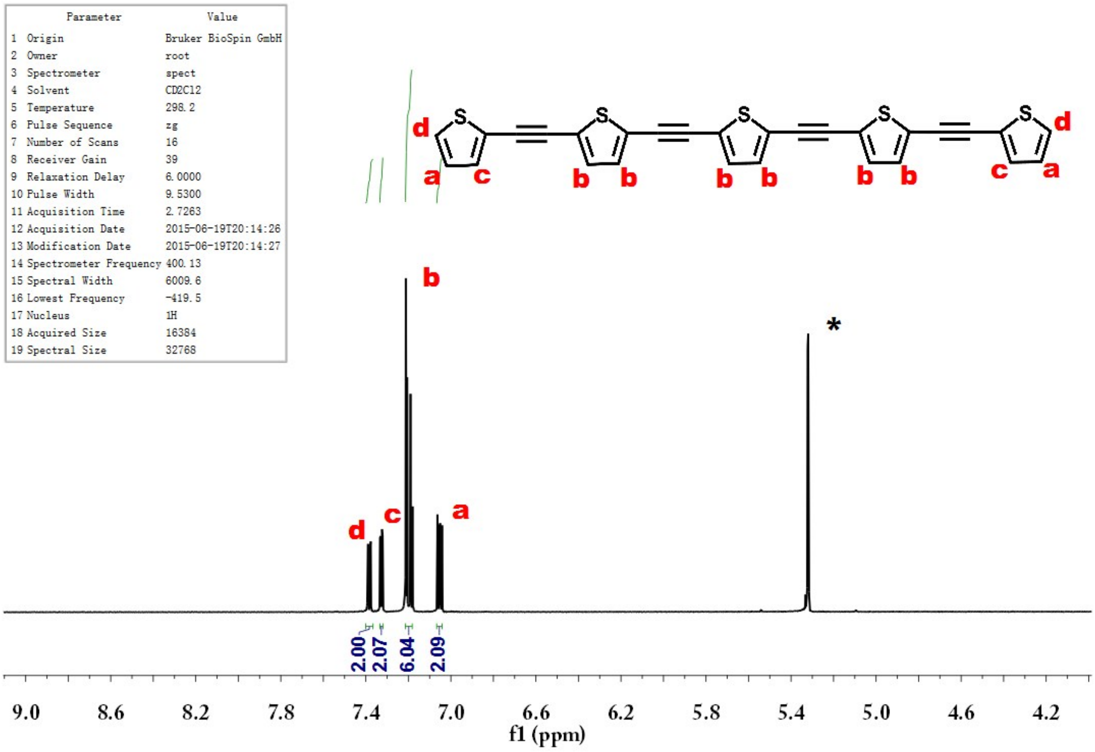

Fig. S7 The ^{1}H NMR spectrum of **4**.

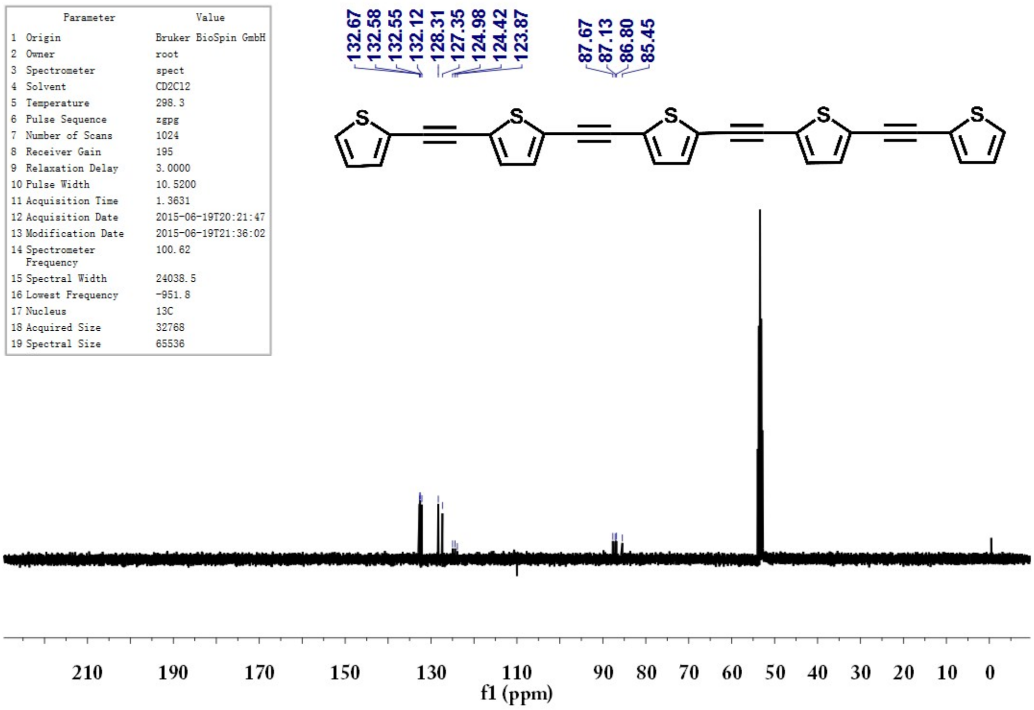

Fig. S8 The ^{13}C NMR spectrum of **4**.

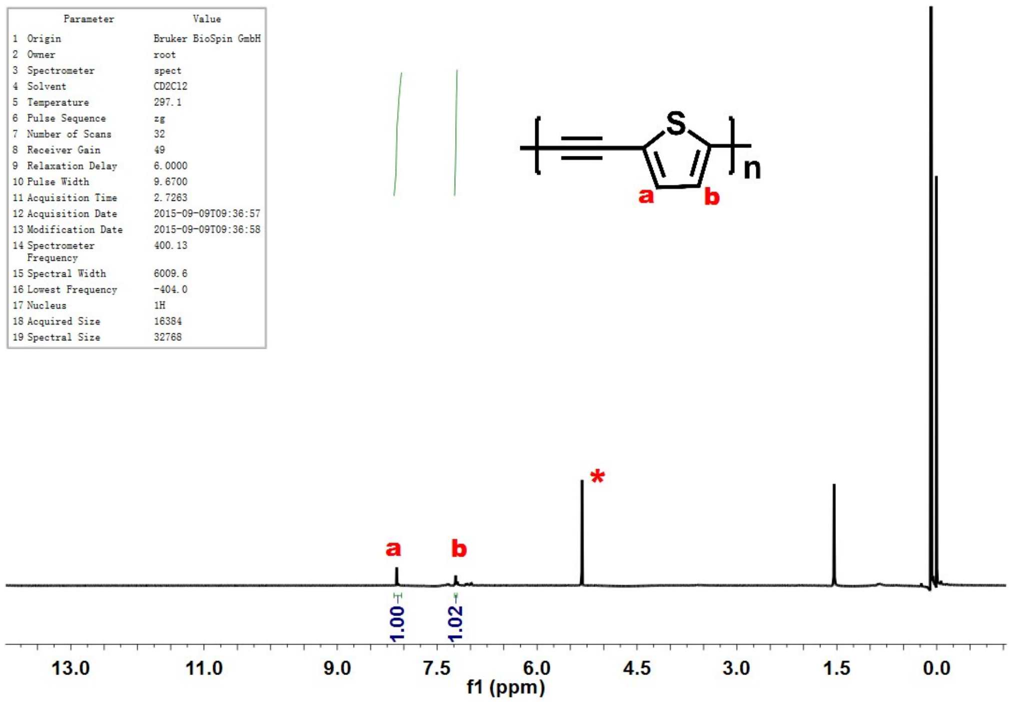

Fig. S9 The ^{1}H NMR spectrum of **PTE**

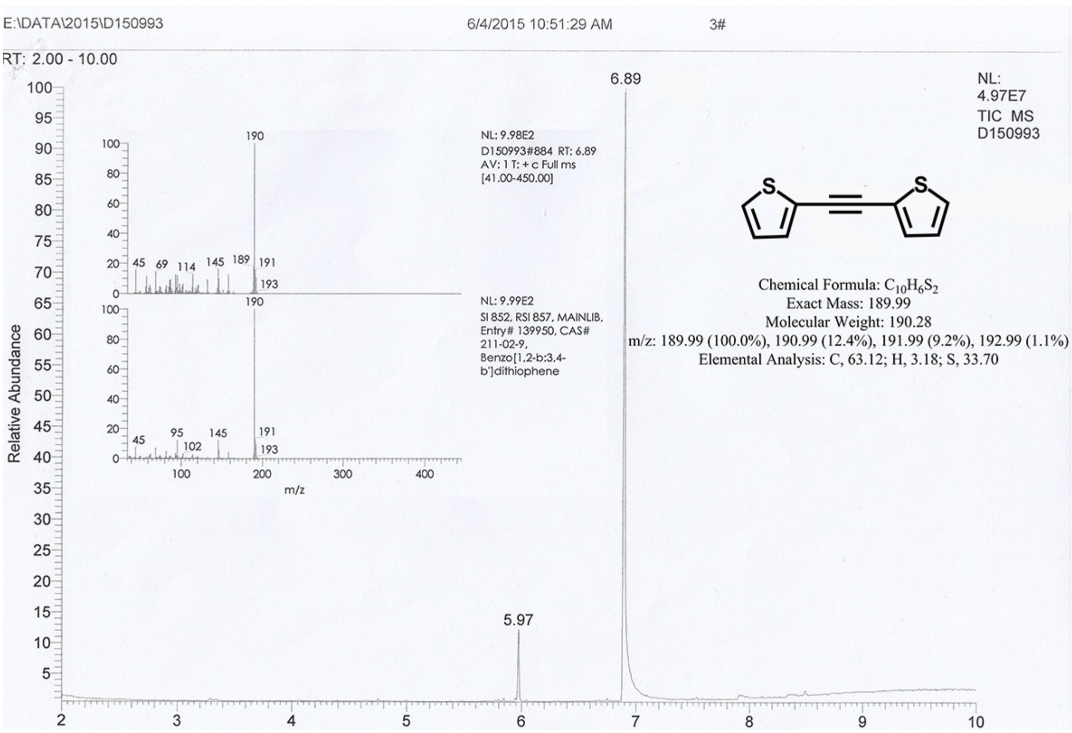

Fig. S10 The MALDI-TOF of **1**.

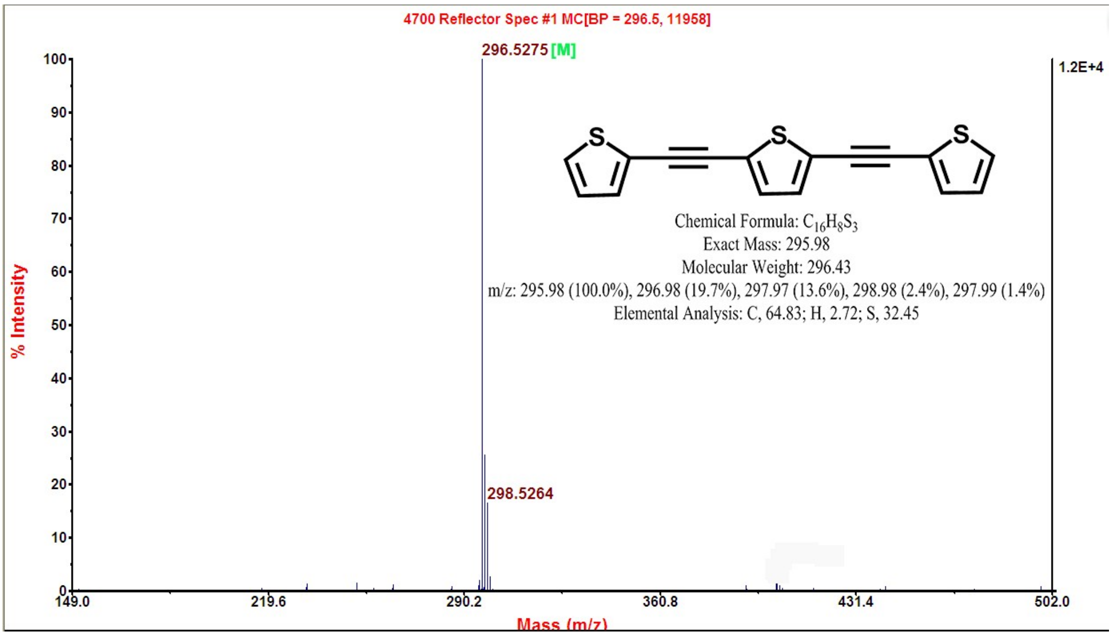

Fig. S11 The MALDI-TOF of **2**.

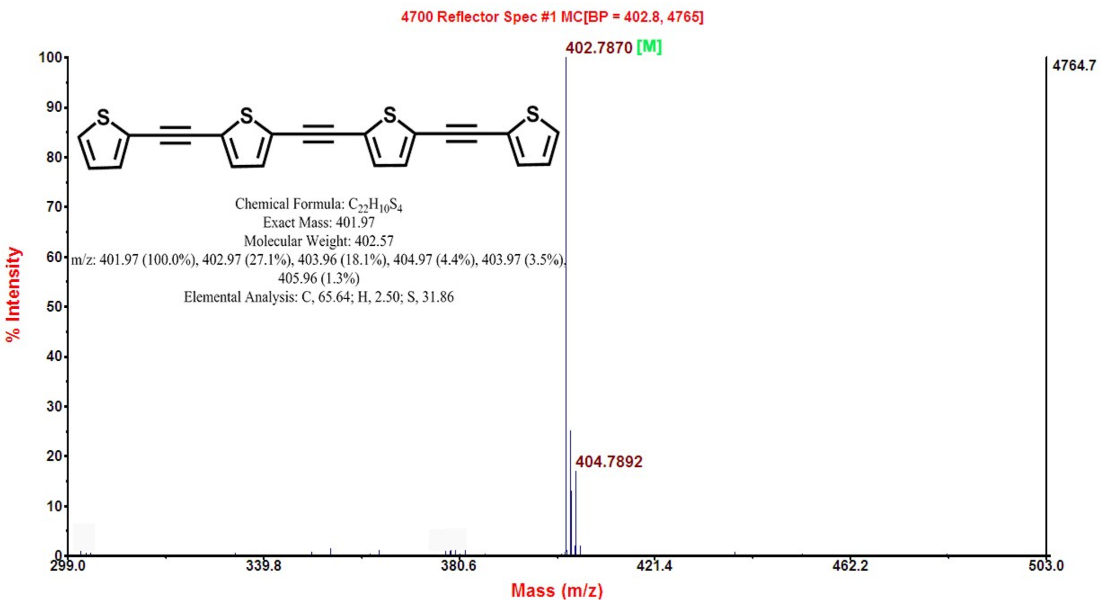

Fig. S12 The MALDI-TOF of **3**.

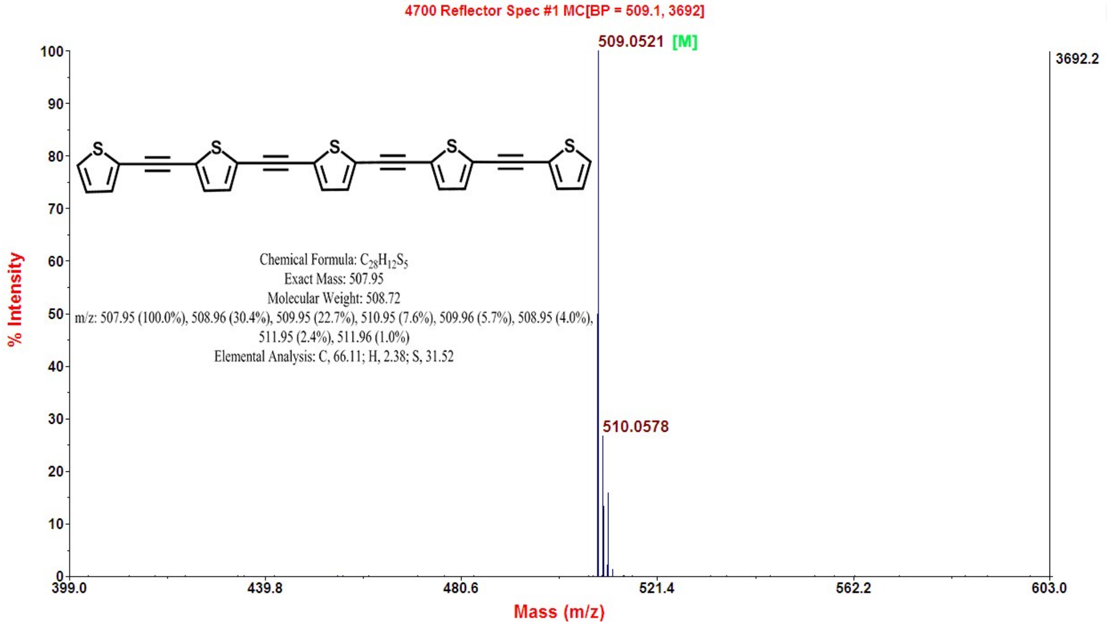

Fig. S13 The MALDI-TOF of **4**.

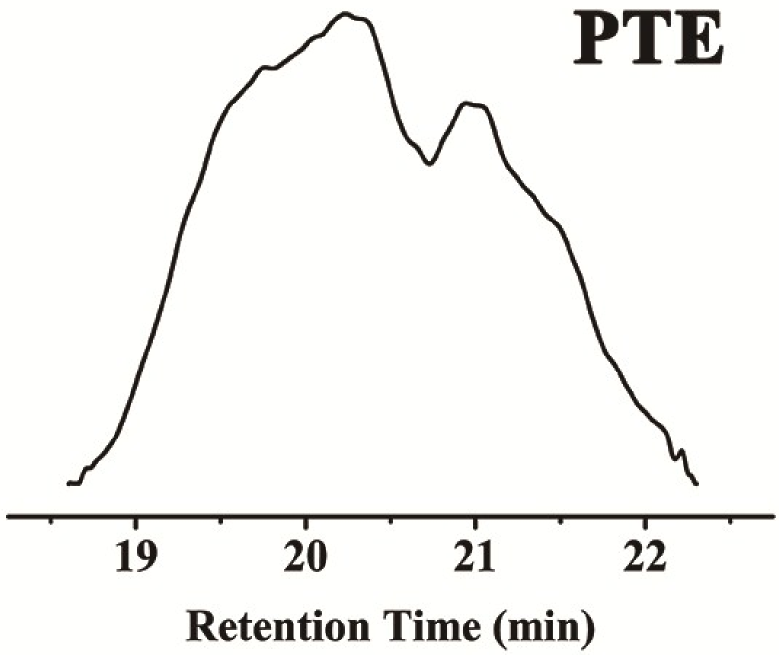

Fig. S14 The GPC data of **PTE**.

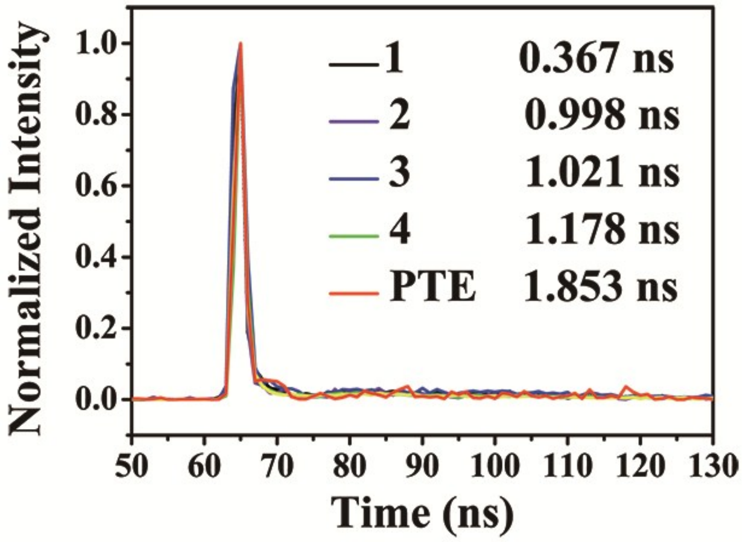

Fig. S15 The fluorescence lifetime of **1-4** and **PTE** in CH_2Cl_2 solutions.

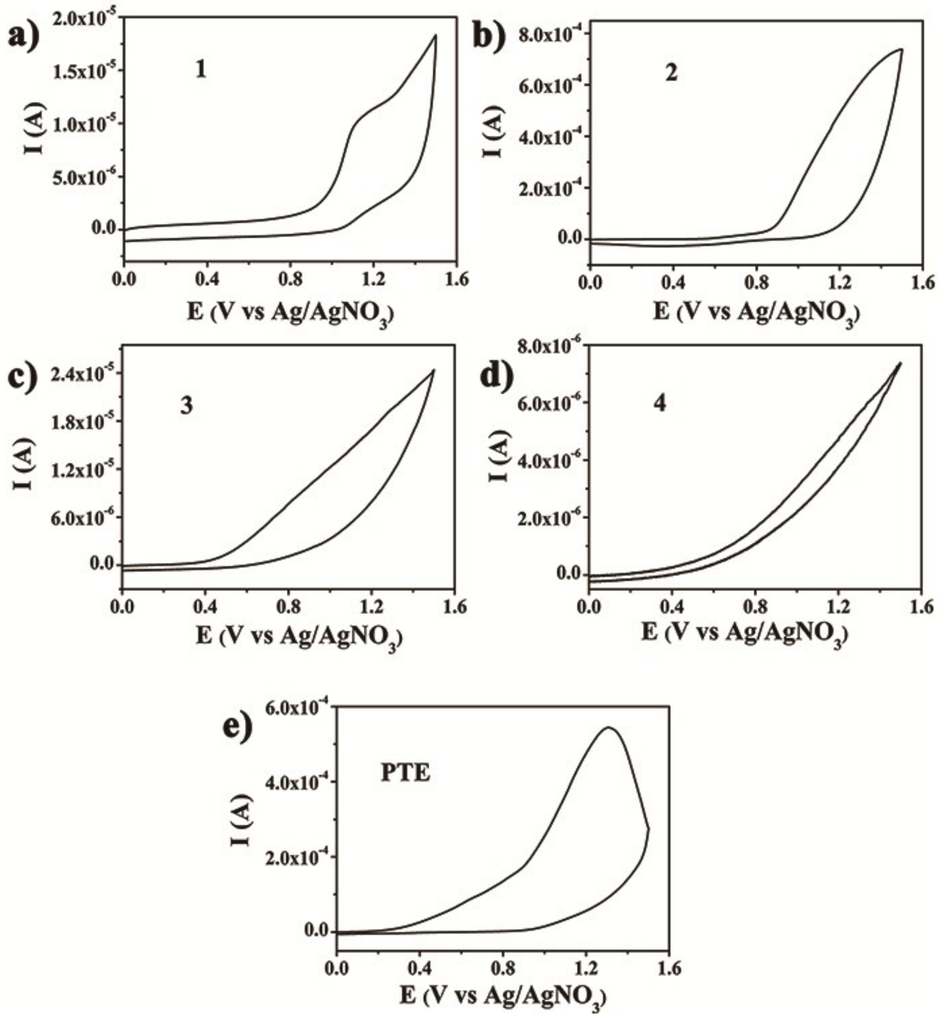

Fig. S16 The CV curves of (a) **1**, (b) **2**, (c) **3**, (d) **4** and (e) **PTE** in CH_2Cl_2 solution.

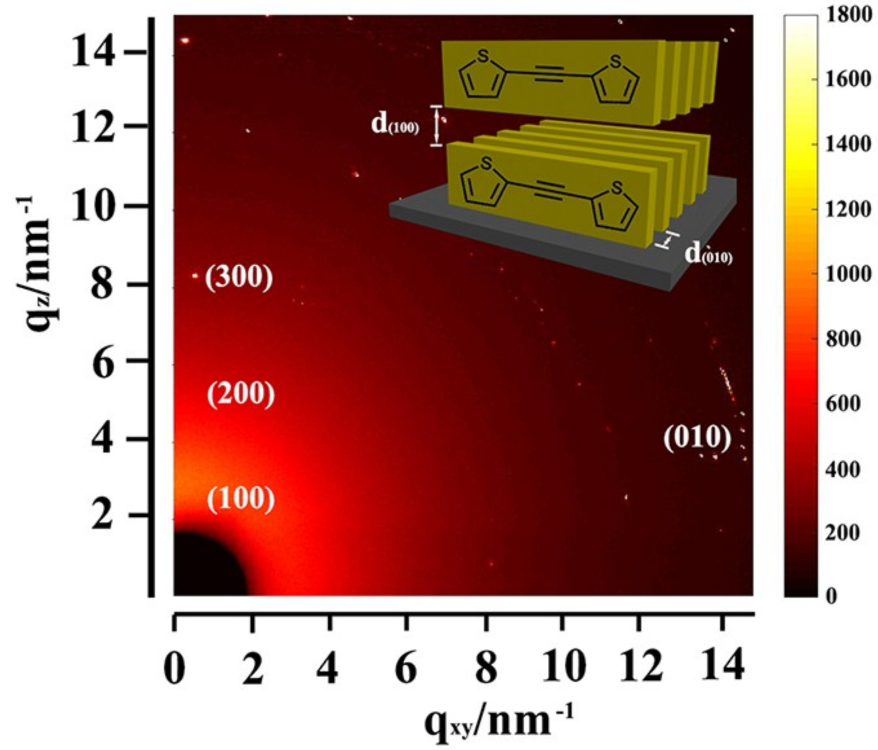

Fig. S17 The 2D-GIXRD patterns of **1**. The inserted model is a schematic diagram of the orientations of the aggregation structure with respect to the substrate in the films.

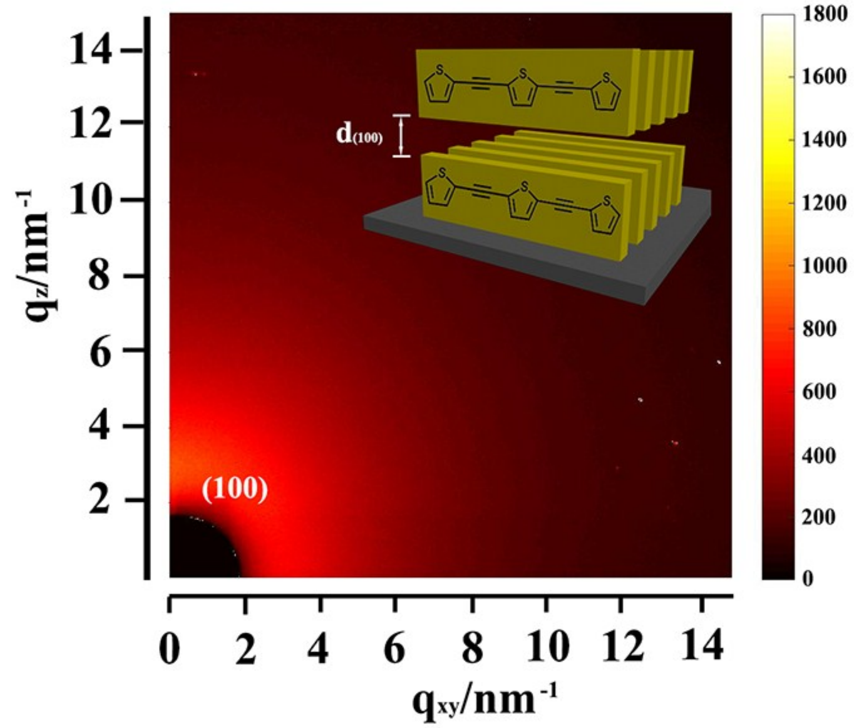

Fig. S18 The 2D-GIXRD patterns of **2**. The inserted model is a schematic diagram of the orientations of the aggregation structure with respect to the substrate in the films.

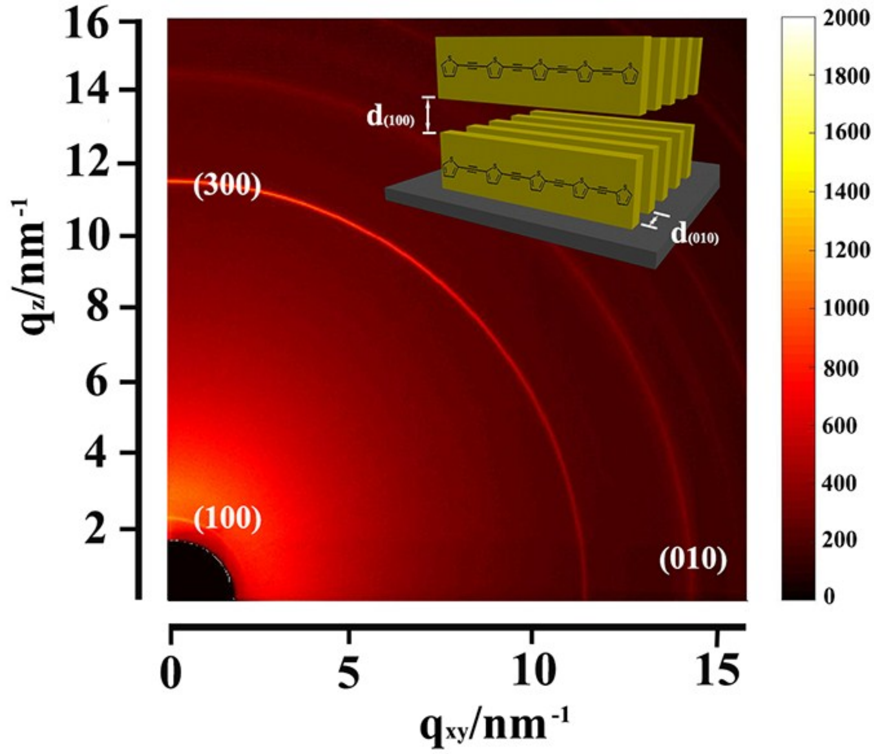

Fig. S19 The 2D-GIXRD patterns of **4**. The inserted model is a schematic diagram of the orientations of the aggregation structure with respect to the substrate in the films.

The detailed calculated procedures for the charge carrier mobility.

According to the obtained V_{th} values and the metal-oxide semiconductor FET formula for the saturation regime, $I_{DS} = \frac{\mu W C_i}{2L}(V_G - V_{th})^2$, the calculations of the charge carrier mobility (μ) are below:

3

I_{DS} =30.79×10^{-6} A， V_G = -6.69 V, V_{DS}=1V, C_i = 20 μF/cm^2, W = 1 mm, L = 1 mm, V_{th} = －1.81 V

μ= 2LI_{DS}/ [WC_i(V_G —V_{th})^2] = 2I_{DS}/[C_i(V_G-V_{th})^2]

= 2×30.79×10^{-7}/[20×10^{-6}×(-6.69＋1.81)^2]

= 0.13 cm^{2}V^{-1}s^{-1}

4

I_{DS} =35.93×10^{-6} A， V_G = -6.23 V, V_{DS}=1V, C_i = 20 μF/cm^2, W = 1 mm, L = 1 mm, V_{th} = －2.14 V

μ= 2LI_{DS}/ [WC_i(V_G —V_{th})^2] = 2I_{DS}/[C_i(V_G-V_{th})^2]

= 2×30.79×10^{-7}/[20×10^{-6}×(-6.69＋1.81)^2]

= 0.22 cm^{2}V^{-1}s^{-1}

PTE

I_{DS} =39.27×10^{-6} A， V_G = -5.27 V, V_{DS}=1V, C_i = 20 μF/cm^2, W = 1 mm, L = 1 mm, V_{th} = －2.22 V

μ= 2LI_{DS}/ [WC_i(V_G —V_{th})^2] = 2I_{DS}/[C_i(V_G-V_{th})^2]

= 2×30.79×10^{-7}/[20×10^{-6}×(-6.69＋1.81)^2]

= 0.42 cm^{2}V^{-1}s^{-1}

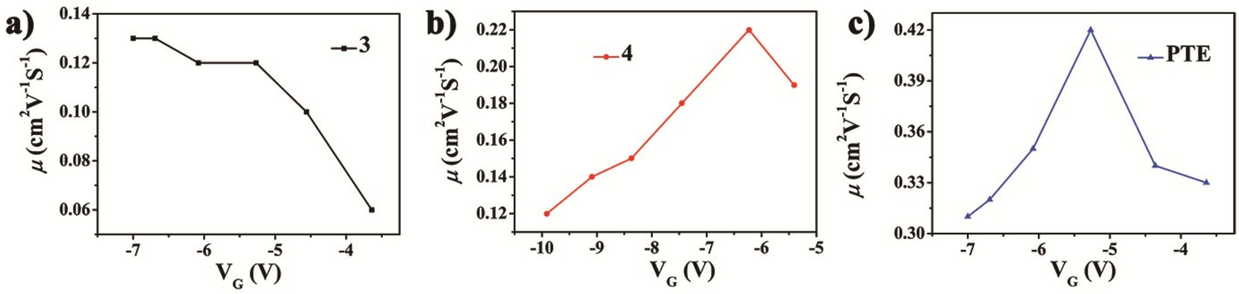

Fig. S20 The mobility plots versus gate voltages for (a) **3**, (b) **4** and (c) **PTE**.

.